Sensors and Materials, Vol. 28, No. 9 (2016) 947–955
MYU Tokyo

S & M 1256

A Novel Spherical Stent Concept for Intracranial Aneurysm

Hao-Ming Hsiao,* Yi-Ping Wang, Yu-Han Cheng,
Tzu-Yuan Lin, and Chien-Erh Lin

Department of Mechanical Engineering, National Taiwan University
No. 1, Sec. 4, Roosevelt Rd., Taipei 10617, Taiwan

(Received December 22, 2015; accepted May 19, 2016)

Keywords: intracranial aneurysm, spherical stent, nitinol, finite element analysis, stroke

Hemorrhagic stroke, caused by the rupture of intracranial aneurysms, is a serious disorder with a high mortality and morbidity. The current standard treatments for intracranial aneurysms include traditional craniotomy and endovascular coiling; however, there are some limitations associated with these two treatments. In this paper, we propose a novel NiTi "spherical stent" concept, the first of its kind in the world. Our proposed spherical stent is able to provide more uniform radial support to an intracranial aneurysm, thereby reducing the risk of rupture. In addition, it can be directly deployed inside the aneurysm in a single step, which significantly shortens the surgery time. Finite element models were developed to predict the behavior of the spherical stent during manufacturing and clinical deployment. A pulsed fiber laser, integrated with a precision X–Y motor stage, was used to make the first prototype of the spherical stent to demonstrate our novel concept.

1. Introduction

An intracranial aneurysm is a cerebrovascular disorder in which a weakness in the wall of a cerebral artery causes localized ballooning of the blood vessel. As an aneurysm grows, it puts pressure on surrounding brain tissues and may eventually rupture, leading to fatal subarachnoid hemorrhage. A subarachnoid hemorrhage is a serious disorder with high mortality and morbidity (Fig. 1).[1–4]

Fig. 1. (Color online) Rupture of an intracranial aneurysm.

*Corresponding author: e-mail: hmhsiao@ntu.edu.tw

ISSN 0914-4935

In traditional craniotomy, an opening is made in the skull under general anesthesia, and the brain is gently retracted to locate the aneurysm. A neurosurgeon then places a tiny clip across the base, or neck, of the aneurysm to stop the blood flow into the aneurysm.[5] Such clips are made of titanium and remain on the artery permanently. The purpose of surgical clipping is to isolate an aneurysm from normal circulation to reduce the risk of rupture without blocking off any small perforating arteries nearby. However, the position, shape, and size of the aneurysm may make it unsuitable for surgery in some cases.

Currently, endovascular coiling is a safe alternative to traditional craniotomy and clip ligation. In 1991, a detachable coil was invented. In this technique, the aneurysm is filled with a coil to block off the aneurysm from the main vessel.[6] The occlusive agent is a detachable platinum coil delivered through a microcatheter positioned within the aneurysm. The entire detachable coil consists of a proximal stainless steel delivery wire welded to an extremely soft coil made of platinum. After the coil is inserted into the aneurysm, it is energized with a low positive direct electric current to detach the platinum coil from the leading wire at the welded junction so that the leading wire can retreat.[7,8] Although it has a high success rate, the endovascular coiling treatment of intracranial aneurysms still has some limitations. When the neck of the aneurysm is over 4 mm wide or the neck/aneurysm length ratio is greater than 0.5, there is a risk that the platinum coil may fall into the blood vessel and cause a stroke.[9]

In this study, we propose a novel NiTi "spherical stent" that can be directly deployed inside an aneurysm to provide uniform radial support to prevent rupture (Fig. 2). This spherical stent concept is the first of its kind in the world. Finite element models were developed to predict the behavior of the spherical stent during manufacture and clinical deployment. These included a series of expansions and heat treatments to achieve the target aneurysm size, and then crimping inside a cylindrical catheter for delivery. Upon arrival at the target site, the spherical stent is released and expands inside the aneurysm. A pulsed fiber laser, integrated with a precision X–Y motor stage, was used to manufacture the first prototype of the spherical stent for demonstration of our novel concept.

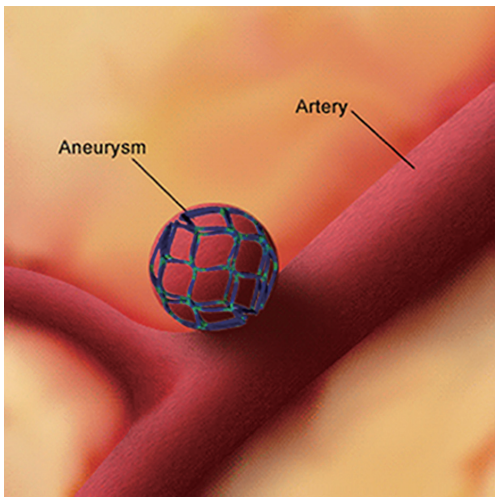

Fig. 2. (Color online) Proposed spherical stent.

2. Materials and Methods

2.1 Spherical stent design

Nitinol (NiTi) is an excellent material for medical devices due to its unique superelasticity and shape-memory properties. Currently, it is widely used in medical engineering, especially in interventional medical devices. The most celebrated application of nitinol is the peripheral self-expanding stent.[10]

In general, cerebral arteries have an average diameter of 2–3 mm,[11] which is smaller than the diameters of most of the vessels in the human body. Therefore, it is critical that a spherical stent be small enough for delivery by micro-catheter. Upon arrival at the target site, the spherical stent is released from the catheter and expands to the size of the aneurysm (3–5 mm). It remains spherical to provide uniform radial support to the aneurysm. The spherical shape also prevents the stent from falling into the blood vessel and potentially causing a stroke.

Designing a spherical stent is a challenging task, as the stent must withstand the large deformations associated with being crimped inside a cylindrical catheter and then expanding to a spherical shape. To achieve this goal, we applied the parametric design concept to the stent design and integrated it with finite element models to evaluate the performance of the spherical stent. With these integrated tools, a modified stent design was accomplished in much less time than with traditional approaches. We first sketched a 2D draft of the spherical stent and then extruded it into a 3D model using SolidWorks software (Dassault Systemes SolidWorks Corp., Massachusetts, USA). Figure 3 shows the 3D model of our spherical stent in its initial cylindrical configuration.

2.2 Finite element models

Computational modeling is a powerful tool in the stent industry due to its ability to give insights into various aspects of stent performance which may consequently improve the clinical outcome.[12–16] In this study, finite element models were developed to evaluate the mechanical integrity of the spherical stent by following these steps:

Step 1: Expand the spherical stent to 2.0, 3.0, 4.0, and 5.2 mm in diameter and anneal the stent after each expansion.

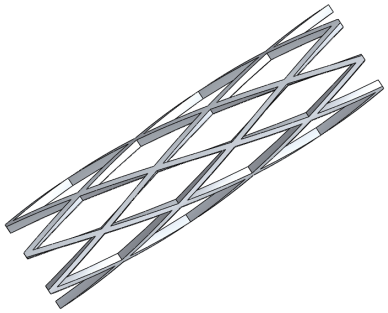

Fig. 3. 3D model of the initial spherical stent.

Step 2: Crimp the spherical stent for delivery inside a cylindrical catheter with an inner diameter of 1.6 mm.
Step 3: Release the spherical stent with a diameter of 5.2 mm inside an aneurysm.

FEA was carried out using the ABAQUS/Standard finite element solver (Dassault Systems Simulia Corp., Providence, RI, USA). To simulate multiple stent expansions and heat treatments during manufacture and subsequent crimping inside a catheter, a sphere with a diameter of 1.0 mm and a cylinder with a diameter of 11.0 mm were added to the model, with the sphere inside the stent and the cylinder outside the stent. For the element selection, the spherical stent body was assigned the cubic element of C3D8I. The properties of the NiTi material were chosen based on the literature.[17] Figure 4 shows the superelastic stress–strain curve of the NiTi. Material parameters in the FEA models were set using the ABAQUS UMAT (user-defined material) subroutine.

2.3 Stent laser cutting

2.3.1 Pulsed fiber laser module

In this study, a laser module consisting of a Rofin 100 W pulsed fiber laser, an Aerotech linear *X*–*Y* motor stage, and a *Z*-direction server motor was assembled and integrated (Fig. 5). The precision stage provided the linear motion and rotation of the hypotube, whereas the *Z*-direction server motor controlled the distance between the laser source and hypotube surface for the optimal focal position. The motor stage accuracy was ±2 μm and ±25 arcsec in the axial and circumferential directions, respectively.

Position synchronized output (PSO), a control algorithm that greatly enhances the efficiency and quality of the laser cutting output, was used to coordinate the linear *X*–*Y* motor stage with the timing of laser firing. The Aerotech A3200 controller allowed us to perform up to 32 axes of synchronized motion control and therefore to accomplish sophisticated laser cutting patterns effortlessly.

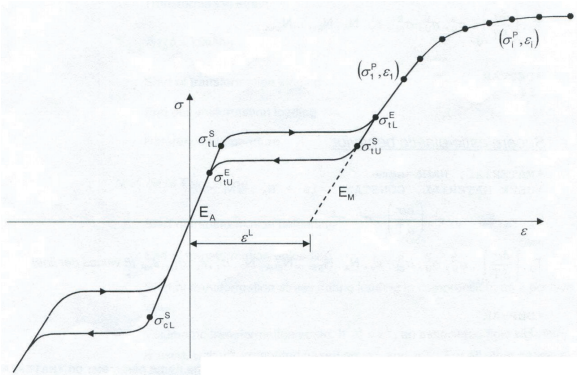

Fig. 4. Stress-strain curve of nitinol.

Fig. 5. (Color online) Integrated pulsed fiber laser module.

In the manufacture of a NiTi stent, a 2D stent drawing is first sketched on the plane and coded into the 3D cylindrical coordinate system by wrapping the 2D sketch around a target cylinder. The coded stent geometry is then fed into the laser module and the stent design pattern is cut onto a seamless hypotube with a diameter of 2.0 mm (Fig. 6).

2.3.2 Input laser parameters

The quality of the laser cutting is controlled by several input parameters such as focal position, pulse repetition rate, and assisted gas pressure. An appropriate laser focal position significantly improves the cutting result. The focal position of our laser module was assessed by measuring the kerf width on the hypotube while adjusting the distance between the laser source and the hypotube surface. The pulse repetition rate is another important laser parameter related to surface roughness and material removal. A higher pulse repetition rate corresponds to a better quality of the cut surface and more effective material removal.

2.4 Heat treatment and surface finishing

Due to the superelastic properties of NiTi, a stent can expand to a large target size when released from a small catheter. To create such superelastic effects, special annealing treatments were applied after laser cutting to progressively shape the stent size/contour to the desired levels and remove the residual stress resulting from each expansion. In this study, the spherical stent was expanded sequentially by the insertion of steel balls of various diameters and then annealed after each expansion in a salt bath at an elevated temperature (Fig. 7).

The high temperatures associated with laser cutting and annealing may create spatter, oxide layers, and other debris that must be removed by further processing. The surface finishing was divided into two major steps: sandblasting, and electropolishing. Sand-blasting was first applied with aluminum oxide particles (37–44 μm) spouted at a pressure of 2 kg/cm^2 for one minute to remove large debris. This step was followed by electropolishing to further improve the surface conditions. The electropolishing solution was mixed with 21% (volume) of perchloric acid and

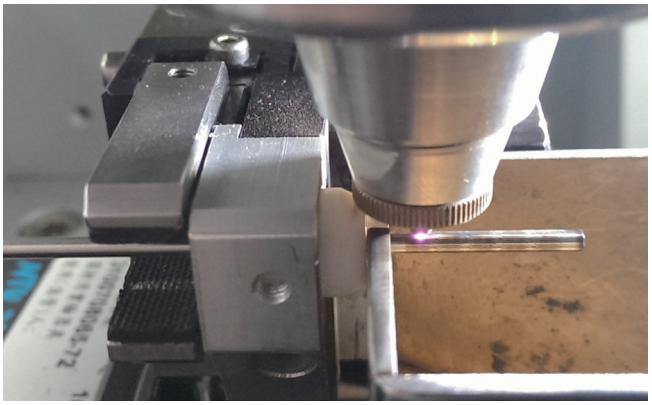

Fig. 6. (Color online) Coded stent geometry cut onto a hypotube.

Fig. 7. (Color online) Spherical stent expansion by insertion of a steel ball.

79% (volume) of acetic acid. The anode was made of a stainless steel flake, and the cathode was made of titanium wire. The electropolishing process was carried out at room temperature in two stages: The spherical stent was polished at 7.7 V for 60 s and then at 11.3 V for an additional 60 s.

3. Results and Discussion

3.1 Novel spherical stent design

The making of a NiTi spherical stent requires an alternating series of expansion and annealing procedures as the stent is formed into its final spherical shape and dimensions. Figure 8 shows the FEA contour plots of the strain distribution during multiple expansions. As shown in Fig. 9, the maximum strain occurred on the inner surface of the most curved regions, with little to none in the neighboring straight portions.

After multiple expansions and annealing treatments were completed, the stent was crimped to a size of 1.6 mm to simulate being constrained inside a catheter. It was then released from the catheter to allow for spring-back to the target diameter of an aneurysm of 5.2 mm. Figure 10 shows the contour plots of the strain distribution upon crimping and after release inside an aneurysm. The crimping appeared to be the most critical stage, as the highest strain values were recorded during this step (Table 1). Overall, our spherical stent was able to withstanding large deformations resulting from crimping inside a cylindrical catheter followed by expansion to a spherical shape.

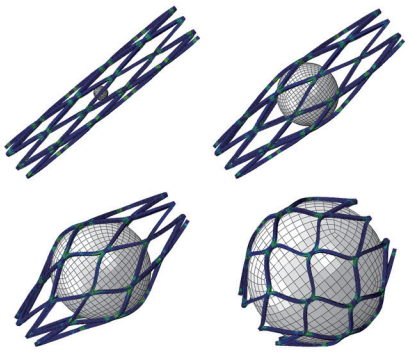

Fig. 8. (Color online) Contours of strain distribution during expansions.

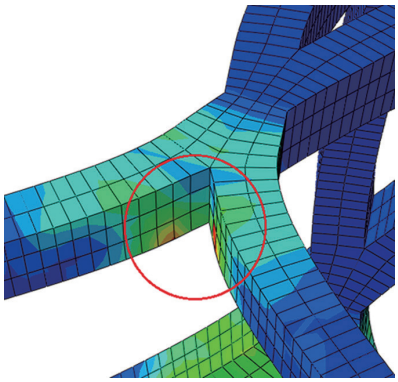

Fig. 9. (Color online) Maximum strain occurred in curved regions.

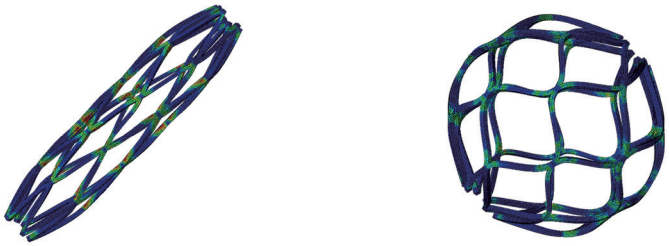

(a) (b)

Fig. 10. (Color online) Contours of strain distribution upon (a) crimping and (b) after release inside an aneurysm.

3.2 Stent laser cutting

The input laser parameters used for cutting spherical stents in this study are listed in Table 2. Optical microscopy was used to measure the kerf width and to observe the surface condition of each stent. Figure 11 shows the relationship of kerf width to *Z*-direction distance between the laser source and the hypotube surface. The smallest kerf width was achieved by precisely focusing the laser sweet spot on the hypotube surface. The kerf width could be reduced to 23.2 μm at a *Z*-direction distance of 0.37 mm. When the *Z*-direction distance was between 0.27 and 0.51 mm, the laser beam was able to penetrate through the hypotube, resulting in successful cutting within a focal-depth range of 0.24 mm in the *Z*-direction.

Figure 12 shows SEM images of two cutting results at different pulse repetition rates. A higher pulse repetition rate corresponds to a better quality of surface cut and more effective material removal [Fig. 12(b)], whereas poor cutting may cause energy to accumulate and form larger heat-affected zones [Fig. 12(a)].

3.3 Heat treatment and surface finishing

After laser cutting, the stent was expanded progressively to the desired size/contour and annealed multiple times in a salt bath at 500 °C for 250 s. Figure 13 shows the prototype of our spherical stent after laser cutting and shaping. The stent surface was then sandblasted and electropolished to achieve a mirror-like finish, as shown in Fig. 14. This is the world's first spherical stent prototype for the demonstration of our novel design.

Table 1
Maximum strain during manufacturing and deployment procedures.

Manufacturing/deployment	Maximum strain
Expand to 2.0 mm	0.1%
Expand to 3.0 mm	4.6%
Expand to 4.0 mm	6.5%
Expand to 5.2 mm	9.1%
Crimp to 1.6 mm	10.0%
Release to 5.2 mm	0.3%

Table 2
Laser parameters used for cutting spherical stents.

Laser cutting parameters	Value
Average power	51 W
Pulse repetition rate	60 kHz
Pulse width	15 μs
Cutting speed	3 mm/s
Gas	Argon
Gas pressure	12 bar

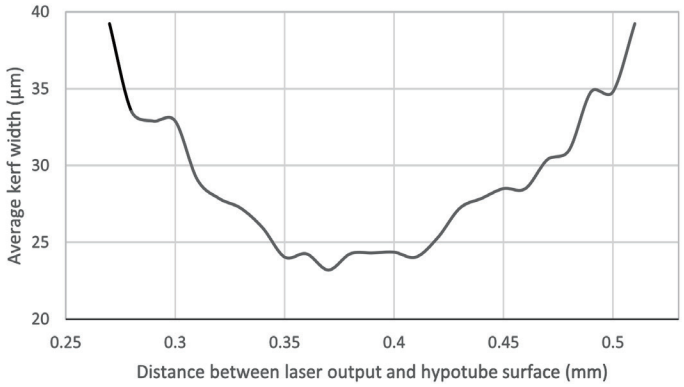

Fig. 11. Kerf width vs *Z*-direction distance between the laser source and hypotube surface.

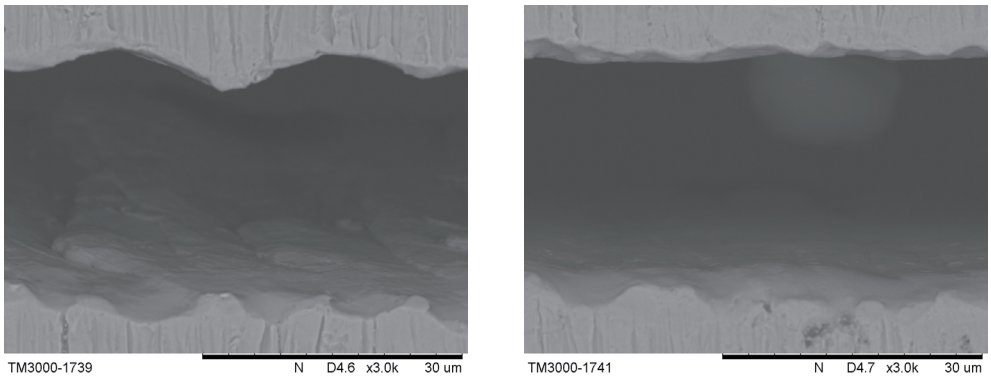

(a) (b)

Fig. 12. SEM pictures of (a) poor vs (b) good laser cutting quality.

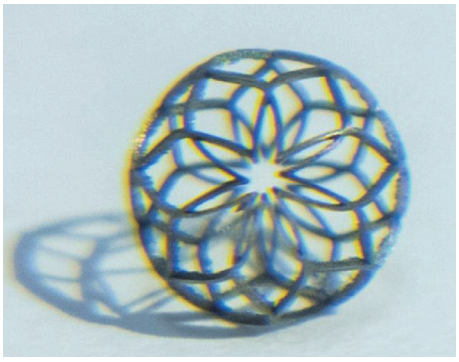

Fig. 13. (Color online) Spherical stent prototype after laser cutting and shaping.

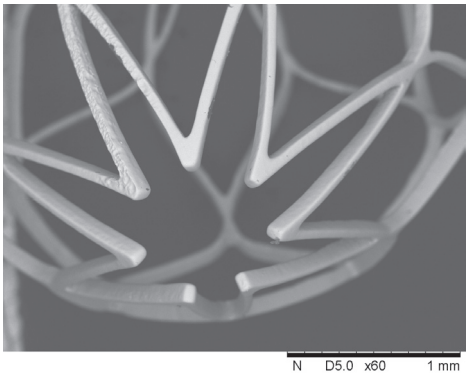

Fig. 14. SEM image of spherical stent prototype after sandblasting and electropolishing.

4. Conclusions

In this paper, we propose a novel NiTi "spherical stent", the first of its kind in the world. Our proposed spherical stent is able to provide uniform radial support to an intracranial aneurysm, thereby reducing the risk of rupture. We applied the parametric design concept to the stent and integrated it with FEA models to evaluate the performance of the spherical stent during manufacturing and deployment. A pulsed fiber laser integrated with a precision *X*–*Y* motor stage was used to make the first spherical stent prototype for demonstration of our novel design.

Acknowledgements

This research was supported by the Ministry of Science and Technology in Taiwan through Grants MOST-105-2221-E-002-092-MY3 and MOST-104-2622-E-002-006-CC1. The authors are grateful for the support and help received.

References

1 J. M. Wardlaw and P. M. White: Brain **123** (2000) 205.
2 A. P. Lozier, E. S. Connolly Jr., S. D. Lavine, and R. A. Solomon: Stroke **33** (2002) 2509.
3 J. L. Brisman, J. L. Song, and D. W. Newell: N. Engl. J. Med. **355** (2006) 928.
4 V. L. Roger, A. S. Go, and D. M. Lloyd-Jones: Circulation **125** (2012) 188.
5 R. A. Solomon, M. E. Fink, and J. Pilespellman: J. Neurosurg. **80** (1994) 440.
6 G. Guglielmi, F. Viñuela, J. Dion, and G. Duckwiler: J. Neurosurg. **75** (1991) 8.
7 A. F. Zubillaga, G. Guglielmi, F. Viñuela, and G. R. Duckwiler: AJNR Am. J. Neuroradiol. **15** (1994) 815.
8 F. Viñuela, G. Duckwiler, and M. Mawad: J. Neurosurg. **86** (1997) 475.
9 H. Dinc, M. H. Ozturk, A. E. Sari, E. Cakir, G. Gazioglu, and K. Kuzeyli: Diagn. Interv. Radiol. **19** (2013) 165.
10 T. W. Duerig, A. Pelton, and D. Stöckel: Mater. Sci. Eng. **273** (1999) 149.
11 S. B. Pai, R. N. Kulkarni, and R. G. Varma: Neurol. Asia **10** (2005) 21.
12 H. M. Hsiao, Y. H. Chiu, K. H. Lee, and C. H. Lin: Comput. Aided Des. **44** (2012) 757.
13 C. Hopkins, P. E. McHugh, N. P. O'Dowd, Y. Rochev, and J. P. McGarry: Comp. Mater. Sci. **80** (2013) 104.
14 H. M. Hsiao and M. T. Yin: Biomed. Microdevices **16** (2014) 133.
15 H. M. Hsiao, S. Prabhu, A. Nikanorov, and M. Razavi: J. Med. Devices **1** (2006) 113.
16 H. M. Hsiao, Y. H. Chiu, T. Y. Wu, J. K. Shen, and T. Y. Lee: Med. Eng. Phys. **35** (2013) 884.
17 T. M. Pham, M. DeHerrera, and W. Sun: Mechanics of Biological Systems and Materials, Vol. 2, Ed. T. Proulx (Springer New York, New York, 2011) pp. 1–10.